Available online at www.sciencedirect.com
ScienceDirect
Trans. Nonferrous Met. Soc. China 28(2018) 700−710
Transactions of Nonferrous Metals Society of China
www.tnmsc.cn

Parameter optimization of microwave sintering porous Ti−23%Nb shape memory alloys for biomedical applications

Mustafa K. IBRAHIM[1], E. HAMZAH[1], Safaa N. SAUD[2], E. M. NAZIM[1], A. BAHADOR[1]

1. Faculty of Mechanical Engineering, Universiti Teknologi Malaysia, 81310 UTM Johor Bahru, Johor, Malaysia;
2. Faculty of Information Sciences and Engineering,
Management & Science University, 40100 Shah Alam, Selangor, Malaysia

Received 13 March 2017; accepted 26 May 2017

Abstract: Porous Ti−23%Nb (mole fraction) shape memory alloys (SMAs) were prepared successfully by microwave sintering with excellent outer finishing (without space holder). The effects of microwave-sintering on the microstructure, phase composition, phase-transformation temperature, mechanical properties and shape-memory effect were investigated. The results show that the density and size of porosity vary based on the sintering time and temperature, in which the smallest size and the most uniform pore shape are exhibited with Ti−23%Nb SMA after being sintered at 900 °C for 30 min. The microstructure of porous Ti−Nb SMA consists of predominant α'', α, and β phases in needle-like and plate-like morphologies, and their volume fractions vary based on the sintering time and temperature. The β phase represents the largest phase due to the higher content of β stabilizer element with little intensities of α and α'' phases. The highest ultimate strength and its strain are indicated for the sample sintered at 900 °C for 30 min, while the best superelasticity is for the sample sintered at 1200 °C for 30 min. The low-elastic modulus enables these alloys to avoid the problem of "stress shielding". Therefore, microwave heating can be employed to sinter Ti-alloys for biomedical applications and improve the mechanical properties of these alloys.

Key words: biomedical Ti−23%Nb alloy; microwave sintering; microstructure; transformation temperature; mechanical properties

1 Introduction

Titanium-based alloys are characterized by excellent corrosion resistance, good ductility and high yield strength; consequently, they are widely used for biomedical applications as human-body implants including hip joints, medical devices and dental implants [1,2]. Among many shape memory alloys (SMAs), Ti–Ni SMAs have been widely utilized for biomedical applications. However, the toxicity and hypersensitivity of Ni have influenced the development of Ni-free shape memory alloys [3] that are non-toxic and good biocompatible elements such as Nb and Ta [4−6]. Therefore, TiNb-based alloys are expectable to be used to biomedical parts due to their low elastic modulus, superior biocompatibility [7,8], superelasticity and good shape memory behaviour [3]. Being able to use powder metallurgy is vital due to the ability to produce near-net-shape components without requiring any deformation and machining operations [9−13]. Ti−Nb alloys can be fabricated by powder metallurgy through several methods including conventional sintering [14,15], metal-injection moulding [16−18], self-propagating high-temperature synthesis [19], hot-isostatic pressing [20], spark-plasma sintering [14,21,22], and microwave sintering. The microwave sintering technique is a relatively new method to prepare Ti−Nb alloys, and it is considered a new sintering method for metals, composites, ceramics and semiconductors [23−25]. Overall, microwave sintering has several advantages such as enhanced diffusion process, reduced energy and sintering-process time, rapid heating rates, and improved mechanical and physical properties [23,24]. The presence of pores that reduce the elastic modulus of porous-titanium alloys [26−28] also allows the implant cells to grow into the pores and integrate with the host tissue [28−30]. This reduced elastic modulus diminishes the effect of "stress shielding", which is generated due to the large mismatch of elastic moduli between the implant materials (>100 GPa) and hard tissue (<20 GPa). The "stress shielding" may cause resorption of these hard

Corresponding author: E. HAMZAH; E-mail: esah@fkm.utm.my
DOI: 10.1016/S1003-6326(18)64702-8

tissues, loosen the implants and finally lead to implantation failure [31−33]. Several studies used the space-holder method for producing porous Ti-based alloys [34−38]. There are also some studies on using space holder and sintering methods to produce foam structures of different metal powders [39−41]. The main problem of using the space-holder method is removing this space holder material from the compacted parts during the sintering process [42]. The space holder materials should be removed carefully to prevent distortion and collapsing of the compacted powders. Moreover, the contamination that occurs due to the presence of oxygen, nitrogen and hydrogen in these materials, which are dissolved in titanium or titanium alloys via increasing temperature during the sintering process, adversely impacts mechanical properties [36]. The main aim of this research is to optimize microwave sintering parameters on the microstructure, mechanical and shape memory properties of Ti−23%Nb (mole fraction) for biomedical applications.

2 Experimental

The raw materials are titanium powder (99.5% in purity and 150 μm in particle size) and niobium powder (99.85% in purity and 74 μm in particle size), and Ti−23%Nb. These powders were mixed using a planetary ball mill (Retsch PM100) for 1 h at a rotating speed of 300 r/min. Ball to powder mass ratio is 4:1 to homogenize the mixture of the powders. Ti−23%Nb powders were converted to pellets (*d*25 mm × 10 mm) by cold-pressing under a uniaxial pressure of 23 MPa for 5 min. Then, these green samples were microwave sintered either at 900, 1000 or 1200 °C for 10 or 30 min at a heating rate of 30 °C/min and furnace cooling to 250−300 °C, followed by water cooling (during furnace cooling, the cylindrical stainless steel 304 was under water cooling). The cooling rate at all parameters showed a small range of 8−9 °C/min. The microwave machine was HAMiLab-V3, SYNOTHERM Corp. Afterwards, Ti−23%Nb microwave-sintered samples were machined by electrical-discharge machining wire and cut to dimensions of 7 mm × 7 mm × 14 mm for the microstructure characterization and compression test and 10 mm × 10 mm × 20 mm for the shape-memory test, according to the standards of ASTM E9-09. Figure 1 presents the schematic diagram of microwave sintering pot consisting of infra-red pyrometer, outer water-cooled cylindrical stainless steel 304, insulation cylindrical cover made from cotton fibres, alumina crucible, rotator motor, small circular opening on the cover of the cylindrical stainless steel 304 used to approach the samples during sintering, which is covered by a sieve to prevent the microwaves from leaving the cylindrical stainless steel and glass, and silicon carbide used as auxiliary heat material. The microwaves were produced by two magnetrons, which were set to be 4.5 kW and 2.45 GHz. The temperature of the samples during sintering was measured by a Fluke Raytek infra-red pyrometer through the openings in the insulation cylindrical cover and alumina crucible, which is possible since infra-red rays can pass through the setup to reach the sample. The silicon carbide was used with a mass of 18−20 g and placed in an alumina crucible with a square top view and internal dimensions of 8.8 cm in length and width and 3.2 cm in height.

The relative density was tested by the Archimedes-drainage method. The optical microscopy (Nikon microscope) was used to determine the average pore size by using software called “iSolution DT”. The microstructure was analyzed by SEM (SEM, Hitachi, model S−3400N). The pore size, pore shape, pore

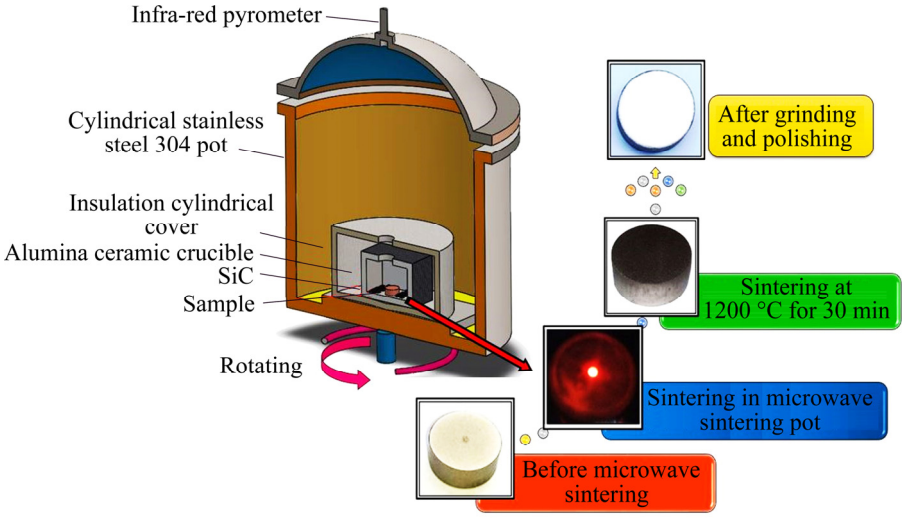

Fig. 1 Schematic diagram of microwave sintering pot

distribution, grain size, volume fraction of the needles and the plates were observed by Imagej software. The phase composition of Ti−23%Nb samples was characterized by X-ray diffraction (D5000 Siemens X-ray diffractometer) fitted with a Cu K_α X-ray source with a locked coupled mode, a 2θ range between 20° and 90° and a scanning step of 0.05 (°)/s. The phase transformation temperatures of these alloys were identified using a differential scanning calorimeter (DSC Q200, TA Instrument) under heating and cooling rates of 10 °C/min using TA Instrument software. The compression test was performed at room temperature using an Instron 600 DX-type universal testing machine and operated at an extension rate of 0.5 mm/min. The microhardness was measured by Vickers hardness test (Matsuzawa Vicker) using 30 kg force for 20 s, and the test was performed at room temperature. The shape memory effect (SME) test was performed using an Instron 600 DX-type universal testing machine, which operated with the special-program parameters according to the SME test, and the loading−unloading cycle compressive test was performed at a strain of 4%. The tests were performed at human body temperature (37 °C), which is below the martensite start temperature (M_s), while below this temperature, the samples would be able to obtain shape recovery. Then, the deformed samples that still had an unrecoverable shape were heated above the austenite finish temperature at 200 °C for 30 min, followed by water quenching to recover the residual strain (ε_r). After the cooling process, the recovered shape was attributed to the transformation of the detwinned martensite to the austenite phase, which had been termed as transformation strain (ε_t).

3 Results and discussion

3.1 Microstructure characterization

The relative density of Ti−23%Nb samples has a small range of 74%−78%, and the density decreased gradually with increasing sintering time and temperature. Figure 2 shows the optical micrographs of Ti−23%Nb samples sintered with different parameters of microwave

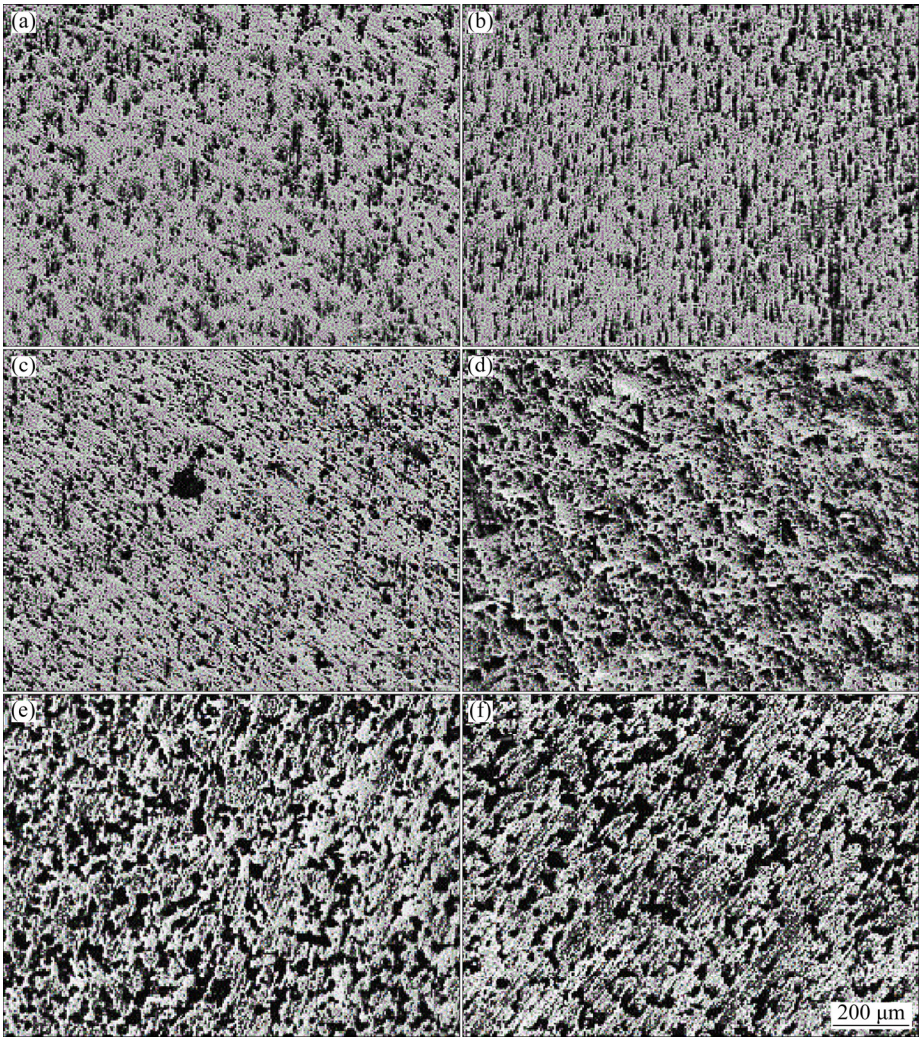

Fig. 2 Optical micrographs of Ti−23%Nb samples sintered at 900 °C for 10 min (a) and 30 min (b), 1000 °C for 10 min (c) and 30 min (d), 1200 °C for 10 min (e) and 30 min (f)

sintering time and temperature. The Ti−Nb sample shown in Fig. 2(b) exhibits the smallest average pore size with a good pore distribution and more uniform pore shape compared with the others samples. Irregular pore shape, non-homogeneous pore distribution, and sharp pore edges act as stress concentration and cause the decrease of mechanical and shape-memory properties, which leads to crack propagation through these pores [43−46]. Table 1 shows the relative density and average pore size of Ti−23%Nb samples. The existence of porosity in the Ti−23%Nb is mainly caused by the inter-diffusion process, and according to Kirkendall effect [10,47], the atoms are able to diffuse during the sintering of solid phase, thus causing the porosity. The diffusion process of niobium atoms into titanium is prominently faster than that of titanium atoms into niobium [48], and due to the unbalance of mass transfer that can result in a pore formation in the niobium-rich region. Figure 1 depicts the Ti−23%Nb samples with all the fabrication steps from the cooled pressed powder until the sample was prepared for microstructure characterization (located on the right side and indicated by the arrow of colored points). After microwave sintering, the Ti−23%Nb samples appeared to have a uniform surface without large cavities or non-uniform shrinkage to satisfy the main principle of powder metallurgy products of producing products without requiring any deformation operation and machining to produce near-net-shape components) [9−13].

Figure 3 illustrates scanning electron microscopy (SEM) images of Ti−23%Nb SMAs. These images

Table 1 Relative density and average pore size of Ti−23%Nb samples

Sintering temperature/°C	Sintering time/min	Relative density/%	Average pore size/μm
900	10	78±4	11.68±0.5
900	30	77±3.7	9.78±0.45
1000	10	76.9±3.7	13.8±0.7
1000	30	75±3.6	13.94±0.7
1200	10	74.2±3.6	19.2±0.9
1200	30	74±3.6	24±1.2

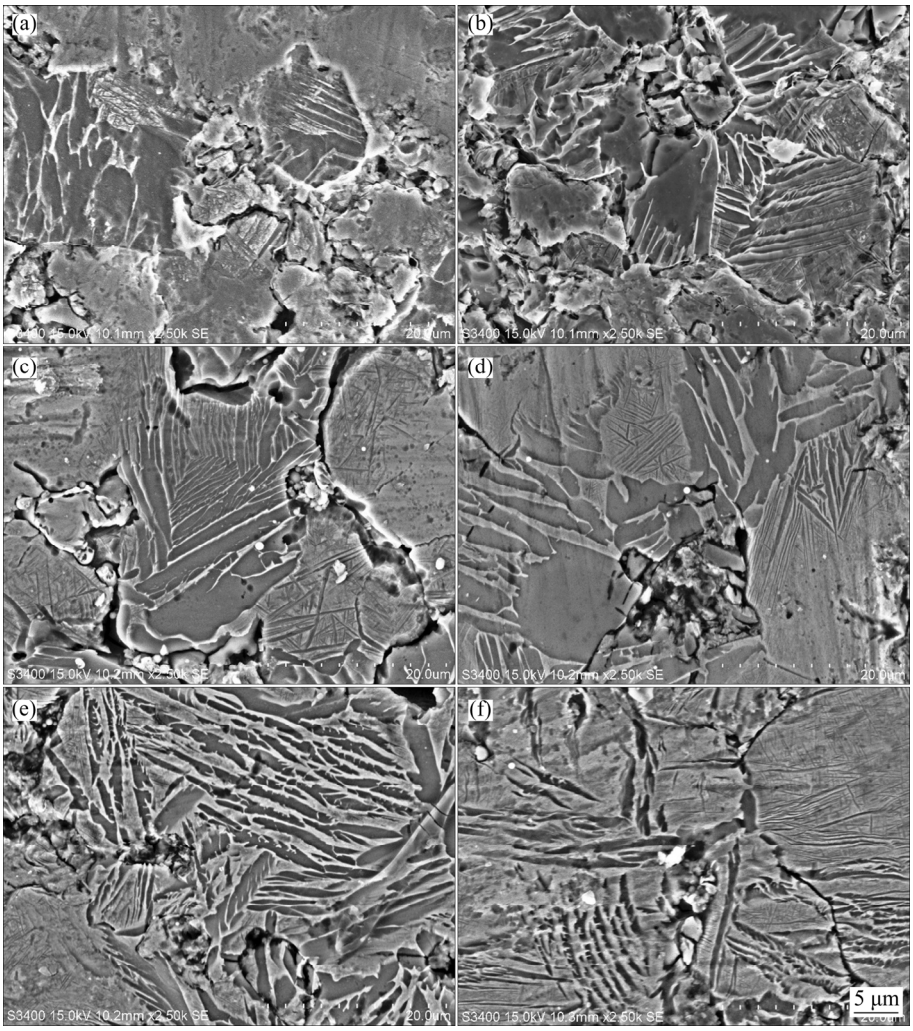

Fig. 3 SEM images of Ti−23%Nb SMAs sintered at 900 °C for 10 min (a) and 30 min (b), 1000 °C for 10 min (c) and 30 min (d), 1200 °C for 10 min (e) and 30 min (f)

illustrate a presence of two types of microstructure morphologies, needle-like and plate-like. Sintering temperature had a larger effect than the sintering time due to the grain size and the volume fraction of the needles and plates. Therefore, the grain size increases with increasing sintering temperature, which may cause diminished mechanical properties because of the crack to propagate easily through the grain boundaries [45,46]. The volume fraction of the needles and plates increased with increasing sintering temperature. KIM et al [49] reported that Ti−(15−35)%Nb (mole fraction) alloys exhibit superelastic and shape-memory properties associated with the β to α'' martensitic transformation, while CHAI et al [50] reported that Ti−(20−24)%Nb alloys exhibit self-accommodation morphologies of the α'' consisting of solid and hollow triangular morphologies and V-shaped morphology. The solid plates of α'' phase were observed in Figs. 3(a) and (b), while the hollow plates (hollow triangular morphology) were observed for samples sintered at 1200 °C, as indicated in Figs. 3(e) and (f), while the α'' plates of the V-shaped morphology can be observed in some parts of the micrographs, as indicated in Fig. 3(c). According to the microstructure and XRD analysis, the β phase increased with increasing sintering temperature and time. Moreover, the increased sintering temperature and time cause dendritic plates-like morphology β_D and needles-like morphology β_N, as indicated in Figs. 3(d)−(f) [51]. For samples sintered at 900 °C, β needle-like morphology similar to spaghetti or irregular lines with α phase between them appeared [52,53]. During cooling, a metastable β phase was retained and other metastable phases (α'', α', α, and ω) were formed from the retained β phase. At low Nb content (i.e., 0.25%<x(Nb)<11%), a supersaturated phase of α' forms martensitically from the β phase during cooling, and regardless of the cooling rate, at higher Nb content (i.e., 11%<x(Nb)<27%) the α'' structure forms from the β phase [54,55], while at the Nb content >27% (mole fraction), the (α+β) structure forms from the β phase [55]. In Ref. [49], the critical content of this alloy shows a scatter due to different cooling rates and impurity levels. Figure 4 shows the elemental mapping of Ti−23%Nb sample sintered at 900 °C for 30 min in Fig. 3(b), which displays the distribution of Ti and Nb in Ti−23%Nb SMA.

Figure 5 demonstrates the XRD patterns of Ti−23%Nb SMAs with different parameters of sintering time and temperatures to verify the presence of β, α'' and α phases in the microstructure and their effect on Ti−23%Nb SMAs. The β phase appears at the planes (110), (200), (211), (112) and (220) at 2θ values of 38.8°, 55.9°, 70°, 76° and 82.7°, respectively. The α'' phase

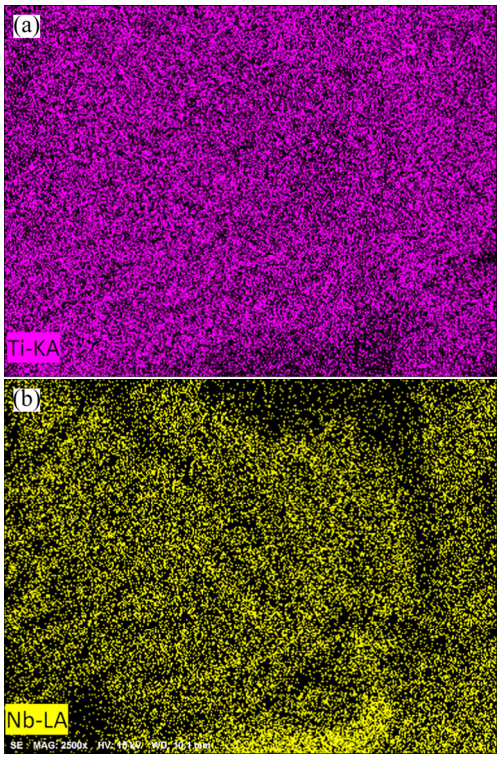

Fig. 4 Elemental mapping of Ti−23%Nb sample sintered at 900 °C for 30 min: (a) Ti; (b) Nb

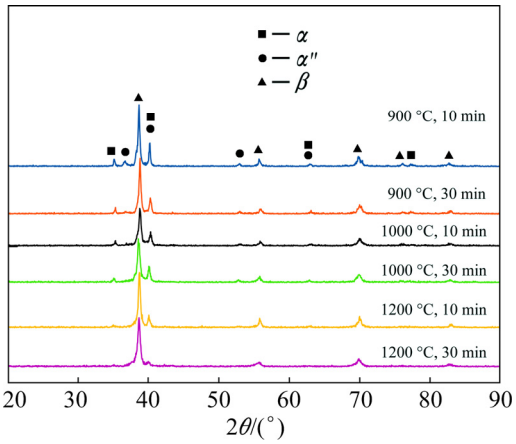

Fig. 5 XRD patterns of Ti−23%Nb SMAs at different microwave sintering parameters

appears at the planes (020), (021), (102) and (130) at 2θ values of 36.7°, 40.2°, 52.7° and 63°, respectively. In addition, the α phase appears at the planes (100), (101), (110) and (201) at 2θ values of 35.17°, 40.2°, 63° and 77.12° [21,56,57]. The shape-memory behaviour and superelasticity of Ti−23%Nb alloy are due to the thermoelastic martensitic transformation between the cubic β parent phase and the orthorhombic α'' martensite phase, as reported by other studies [49,58−60]. The Ti−23%Nb sample, which was sintered at 1200 °C for 30 min, exhibits the minimum intensities of α and α'' phase peaks. The samples exhibit reduced intensities of those peaks with increasing sintering temperature and

time. The composition has the main effect on the microstructure of Ti−Nb alloy due to the type of the phases which were produced during the cooling [54,55], but sintering parameters affect the intensities of these phases [61]. However, the β phase represents the largest phase (see Fig. 3) due to the higher content of β stabilizer element, with small intensities of α and α'' [56].

3.2 Transformation temperature

Figure 6 shows differential scanning calorimeter (DSC) curves of the Ti−23%Nb samples sintered at different parameters of temperature and time. The transformation temperatures are M_s (martensite start temperature), A_s (austenite start temperature), M_f (martensite finish temperature) and A_f (austenite finish temperature). These transformation temperatures were recorded by the directly extrapolating the baseline of the DSC curves by using TA Instrument software. The austenitic transformation peaks were difficult to be detected with increasing the sintering temperature and time in Figs. 6(d)−(f), while martensitic transformation peaks can be observed for all samples. In addition, the martensite start temperature (M_s) was below 105 °C for all samples. Table 2 displays the transformation

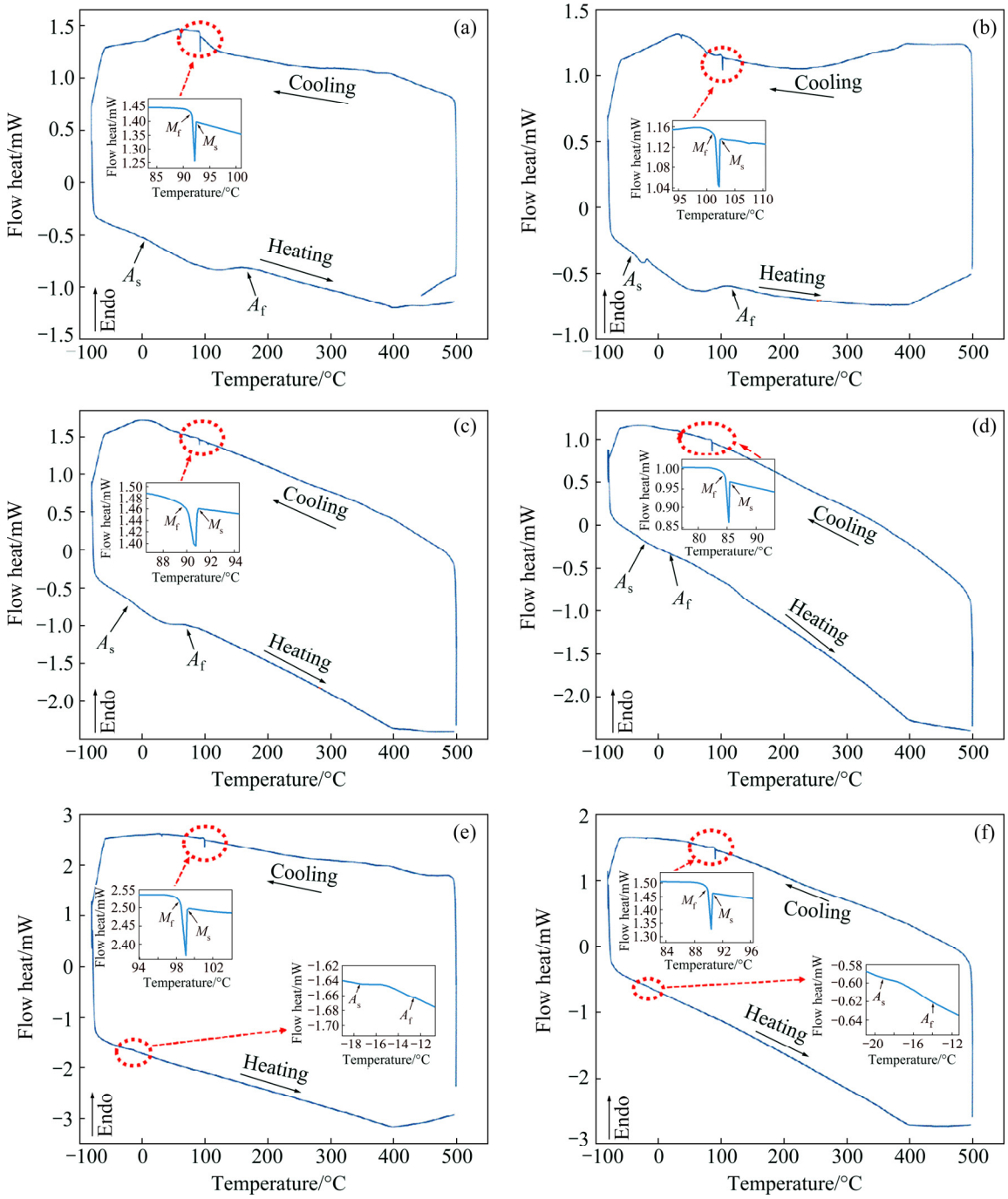

Fig. 6 Differential scanning calorimeter (DSC) curves of Ti−23%Nb samples sintered at 900 °C for 10 min (a) and 30 min (b), 1000 °C for 10 min (c) and 30 min (d), 1200 °C for 10 min (e) and 30 min (f)

Table 2 Transformation temperatures of Ti−23%Nb SMAs at different sintering time and temperatures

Sintering temperature/°C	Sintering time/min	Transformation temperature/°C			
		M_s	M_f	A_s	A_f
900	10	92.62	91	5.94	157
900	30	102.4	100.8	−37	108
1000	10	91.2	89	−13	78
1000	30	85.65	84.2	−15.6	45
1200	10	99.8	98	−17	−10
1200	30	90.8	89.2	−19.3	−14.2

temperatures of Ti−23%Nb SMAs. During heating, the ranges of the A_s to A_f transformation decreased with increasing sintering time and temperature. The DSC result indicates that these SMAs are suitable for biomedical applications, which makes any small load enough for austenite to transform into martensite. The A_f temperature was reduced with increasing sintering time and temperature, enhancing the martensitic transformation at human body temperature.

3.3 Mechanical properties

3.3.1 Stress−strain curves

Figures 7(a) and (b) display the compressive curves of microwave sintered Ti−23%Nb SMAs. The compressive stress−strain curves can be divided into three main regions, as shown in Fig. 7(c) [62]. The first one is a region of the linear-elastic deformation, and its slope is considered as the elastic modulus of these samples, followed by the region of the plastic yield deformation in which a peak stress appears and is considered as the sample's compressive strength. Lastly, the third region in which the rupture occurs is called the rupture region. Table 3 displays the maximum stress (fracture strength), strain at the maximum stress, elastic modulus, and Vickers hardness. The Ti−23%Nb sample sintered at 900 °C for 10 min exhibits the lowest strength and strain maybe due to poor bonding between the powders, and the energy dispersive spectroscopy (EDS) results showed poor diffusion between the Ti and Nb powders for this sample. The sample sintered at 900 °C for 30 min exhibits the maximum stress and strain due to good bonding, good diffusion between the powders and fine grain size. Thus, increasing sintering temperature causes increased grain size and reduced maximum stress and strain due to crack propagation through grain boundaries [45,46] (see Figs. 3(e) and (f)). From Fig. 3 we can observe clearly that the microstructure of the sample in Fig. 3(b) has the smallest grain size compared with all the others samples, which gives this sample the highest fracture strength and strain. The microstructure in Fig. 3(c) shows incomplete bonding with sharp spaces surrounding the atoms that diminish the mechanical properties. The Vickers hardness and elastic modulus increase with increasing sintering time at the same temperature and with increasing temperature at the same sintering time, except the elastic modulus for sample sintered at 1200 °C. The pores and microwave sintering process have the main effect on reducing the elastic modulus [26−28] and hardness.

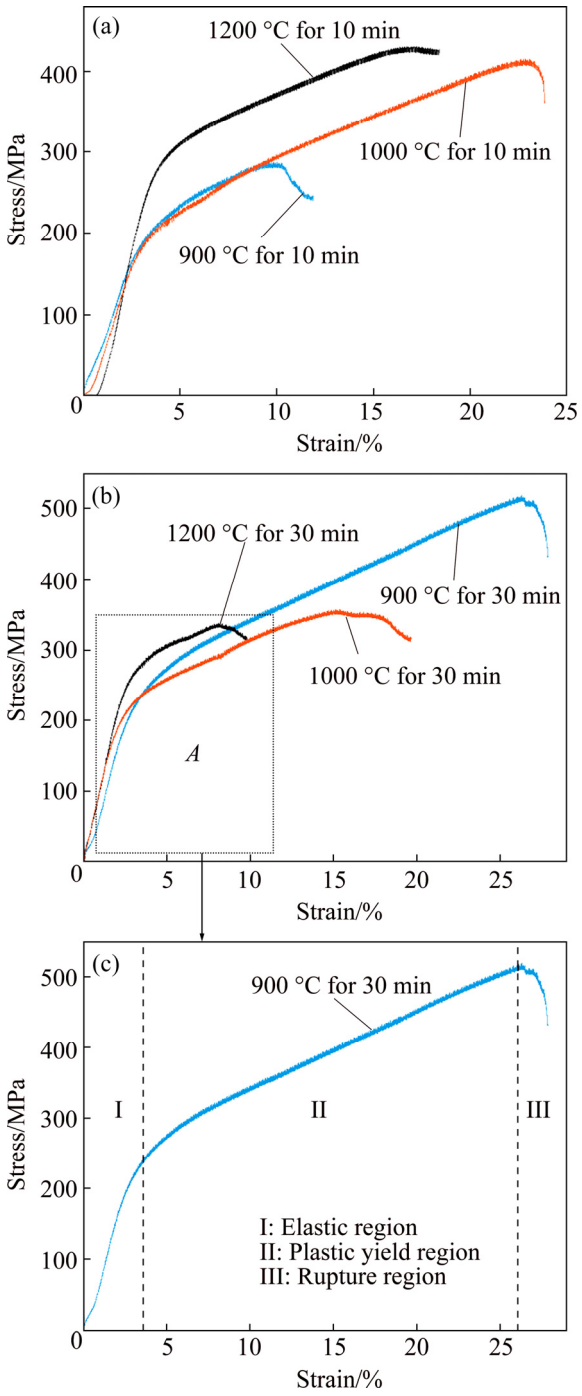

Fig. 7 Compressive stress−strain curves of Ti−23%Nb alloys at different microwave sintering parameters (a, b) and three main regions of stress−strain curve enlargment of zone *A* in Fig. 7(b) of sample sintered at 900 °C for 30 min (c)

3.3.2 Shape-memory effect

The shape-memory effect arises because the martensitic phase can arrange itself into a self-accommodation, finely twinned structure (heterogeneous) with no or little macroscopic strain relative to austenite. Hence, upon cooling from austenitic to martensitic phase, little strain or shape change is usually observed (one-way SME). We call this a self-accommodation form of thermal martensite unless the material or alloy has been heavily processed to have the so-called two-way SME [63]. Figure 8 displays the shape memory behavior of Ti−23%Nb SMAs because of varying the sintering time and temperature. Table 4 displays the maximum stress, shape memory effect, residual strain, and superelasticty. As for the recovery of the residual strain of the compressed samples, after heating the samples above A_f up to 200 °C, this strain recovery of these alloys is due to their SME. The shape memory effect represents the strain recovery. Based on transformation temperature curves in Fig. 6(a)−(f), the M_s of Ti−23%Nb is smaller than 150 °C, so applying the strain at 37 °C (below M_s) makes the Ti−23%Nb samples able to obtain shape recovery. The XRD patterns show that the β phase is the main phase in the sample sintered at 1200 °C for 30 min at ambient temperature, while α and α'' phases are increased with reducing sintering time and temperature. The SME is decreased by increasing the precipitates of the equilibrium α phase [64]. However, the β phase can transform to martensitic α'' phase by adding stress during loading; while during unloading with the release of the stress, the unstable martensitic α'' phase mostly transforms back to the β phase [65]. The constituting phases in these samples were detected by diffraction in transmission. This shape memory behaviour which is

Table 3 Effect of sintering parameters on maximum stress and strain, elastic modulus, and Vickers hardness of Ti−23%Nb alloys

Sintering temperature/°C	Sintering time/min	Maximum strength, σ_{max}/MPa	Strain at σ_{max}, ε_{max}/%	Elastic modulus, E/GPa	Vickers hardness (HV)
900	10	285±14.2	9.88±0.45	6.6±0.33	51.45±2.5
900	30	515±25.7	26.3±1.3	8±0.4	61.7±3
1000	10	411±20.5	22.8±1.1	6.62±0.33	60±3
1000	30	354±17.7	15.24±0.76	8.69±0.43	64±3.2
1200	10	428±21.4	16.8±0.84	9.2±0.46	69±3.4
1200	30	334.6±16.7	8.2±0.41	8.8±0.44	87.4±4.3

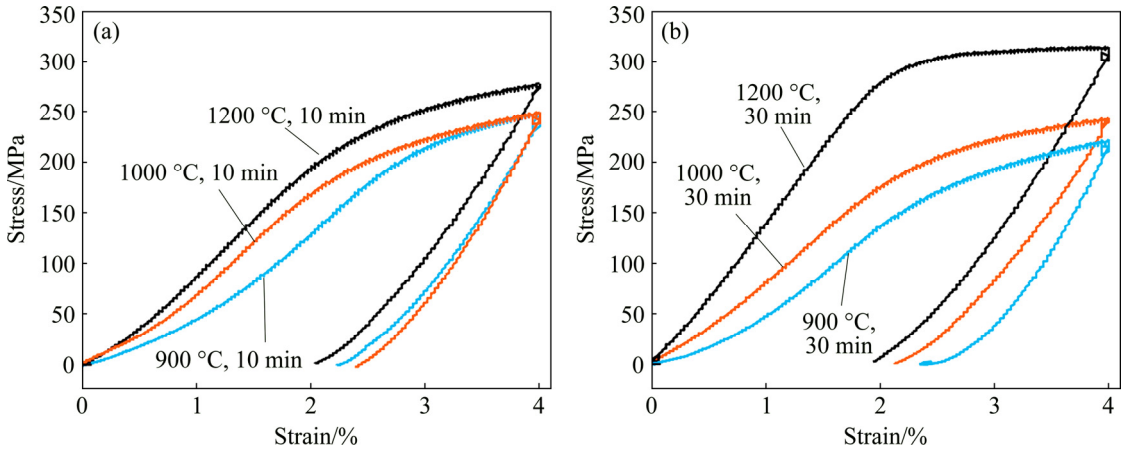

Fig. 8 Stress−strain curves of Ti−23%Nb alloys at human body temperature (37 °C) sintered at different temperatures for 10 min (a) and 30 min (b)

Table 4 Shape memory properties of Ti−23%Nb alloys sintered at different time and temperatures

Sintering temperature/°C	Sintering time/min	Maximum stress, σ_{max}/MPa	Shape memory effect, SME/%	Residual strain, ε_r/%	Superelasticty, SE/%
900	10	248±12.4	0.0005	2.2195±0.11	44.512±2.22
900	30	222±11	0.0015	2.3785±0.11	40.537±2
1000	10	249±12.45	0.0005	2.3995±0.11	40±2
1000	30	243±12.15	0.00014	2.1199±0.1	47±2.3
1200	10	278±13.9	0.0001	2.0299±0.1	49.252±2.4
1200	30	315±15.75	0.0002	1.9398±0.09	51.5±2.5

associated with the β to α'' martensitic transformation may be the reason of obtaining a good shape memory behaviour for the samples sintered at 1200 °C. While the sample sintered at 1000 °C for 10 min shows less superelasticty even from the samples sintered at lower temperature and time, and lower intensities of β phase may be due to the weakness in microstructure because of the non-completed or non-uniform diffusion leaves spaces between the atoms shown in Fig. 3(c).

4 Conclusions

By using the microwave sintering technique, we successfully fabricated the porous Ti−23%Nb SMAs, and investigated the effects of microwave sintering parameters on the microstructure, phase composition, phase transformation temperatures, mechanical properties and shape memory effect of these alloys. Needle-like and plate-like microstructures of Ti−23%Nb SMAs are evidenced. However, the plate-like microstructure is displayed in three morphologies, α'', α', and α phases. Increasing the sintering time and temperature enhances the martensitic transformation due to the gradual decrease of A_f temperatures that allow the martensitic transformation to easily occur at human body temperature. The highest stress and strain were attained for the sample sintered at 900 °C for 30 min due to the highest density, smallest pore size, and uniform pore shape and distribution, while the highest superelasticty was obtained for sample sintered at 1200 °C for 30 min. Our systematic methods for sample preparation and characterization may constitute a basis to produce quality-biocompatible Ti−23%Nb SMAs.

Acknowledgements

The authors would like to thank the Ministry of Higher Education of Malaysia and Universiti Teknologi Malaysia for providing the financial support under the University Research Grant No. Q.J130000.3024. 00M57 and research facilities.

References

[1] LONG M, RACK H. Titanium alloys in total joint replacement—A materials science perspective [J]. Biomaterials, 1998, 19(18): 1621−1639.

[2] HUISKES R, WEINANS H, van RIETBERGEN B. The relationship between stress shielding and bone resorption around total hip stems and the effects of flexible materials [J]. Clinical Orthopaedics and Related Research, 1992, 274: 124−134.

[3] MIYAZAKI S, KIM H, HOSODA H. Development and characterization of Ni-free Ti-base shape memory and superelastic alloys [J]. Materials Science and Engineering A, 2006, 438: 18−24.

[4] WEVER D, VELDHUIZEN A, SANDERS M, SCHAKENRAAD J, van HORN J. Cytotoxic, allergic and genotoxic activity of a nickel−titanium alloy [J]. Biomaterials, 1997, 18(16): 1115−1120.

[5] NIINOMI M. Fatigue performance and cyto-toxicity of low rigidity titanium alloy, Ti−29Nb−13Ta−4.6Zr [J]. Biomaterials, 2003, 24(16): 2673−2683.

[6] LAHEURTE P, PRIMA F, EBERHARDT A, GLORIANT T, WARY M, PATOOR E. Mechanical properties of low modulus β titanium alloys designed from the electronic approach [J]. Journal of the Mechanical Behavior of Biomedical Materials, 2010, 3(8): 565−573.

[7] INAMURA T, HOSODA H, WAKASHIMA K, MIYAZAKI S. Anisotropy and temperature dependence of Young's modulus in textured TiNbAl biomedical shape memory alloy [J]. Materials Transactions, 2005, 46(7): 1597−1603.

[8] MASAHASHI N, MIZUKOSHI Y, SEMBOSHI S, OHTSU N, JUNG T, HANADA S. Photo-induced characteristics of a Ti–Nb–Sn biometallic alloy with low Young's modulus [J]. Thin Solid Films, 2010, 519(1): 276−283.

[9] HEY J, JARDINE A. Shape memory TiNi synthesis from elemental powders [J]. Materials Science and Engineering A, 1994, 188(1): 291−300.

[10] ZHANG N, KHOSROVABADI P B, LINDENHOVIUS J, KOLSTER B. TiNi shape memory alloys prepared by normal sintering [J]. Materials Science and Engineering A, 1992, 150(2): 263−270.

[11] GREEN S, GRANT D, KELLY N. Powder metallurgical processing of Ni−Ti shape memory alloy [J]. Powder Metallurgy, 1997, 40(1): 43−47.

[12] IGHARO M, WOOD J. Compaction and sintering phenomena in titanium−nickel shape memory alloys [J]. Powder Metallurgy, 1985, 28(3): 131−139.

[13] MORRIS D, MORRIS M. NiTi intermetallic by mixing, milling and interdiffusing elemental components [J]. Materials Science and Engineering A, 1989, 110(1): 139−149.

[14] WEN M, WEN C, HODGSON P, LI Y. Fabrication of Ti−Nb−Ag alloy via powder metallurgy for biomedical applications [J]. Materials & Design, 2014, 56: 629−634.

[15] XIONG J, LI Y, WANG X, HODGSON P, WEN C E. Mechanical properties and bioactive surface modification via alkali-heat treatment of a porous Ti−18Nb−4Sn alloy for biomedical applications [J]. Acta Biomaterialia, 2008, 4(6): 1963−1968.

[16] ZHAO D, CHANG K, EBEL T, NIE H, WILLUMEIT R, PYCZAK F. Sintering behavior and mechanical properties of a metal injection molded Ti−Nb binary alloy as biomaterial [J]. Journal of Alloys and Compounds, 2015, 640: 393−400.

[17] ZHAO D, CHANG K, EBEL T, QIAN M, WILLUMEIT R, YAN M, PYCZAK F. Microstructure and mechanical behavior of metal injection molded Ti−Nb binary alloys as biomedical material [J]. Journal of the Mechanical Behavior of Biomedical Materials, 2013, 28: 171−182.

[18] KAFKAS F, EBEL T. Metallurgical and mechanical properties of Ti−24Nb−4Zr−8Sn alloy fabricated by metal injection molding [J]. Journal of Alloys and Compounds, 2014, 617: 359−366.

[19] ALEKSANYAN A, DOLUKHANYAN S, SHEKHTMAN V S, KHASANOV S, TER-GALSTYAN O, MARTIROSYAN M. Formation of alloys in the Ti−Nb system by hydride cycle method and synthesis of their hydrides in self-propagating high-temperature synthesis [J]. International Journal of Hydrogen Energy, 2012, 37(19): 14234−14239.

[20] MA L W, CHUNG C Y, TONG Y, ZHENG Y. Properties of porous TiNbZr shape memory alloy fabricated by mechanical alloying and hot isostatic pressing [J]. Journal of Materials Engineering and Performance, 2011, 20(4−5): 783−786.

[21] TERAYAMA A, FUYAMA N, YAMASHITA Y, ISHIZAKI I, KYOGOKU H. Fabrication of Ti−Nb alloys by powder metallurgy process and their shape memory characteristics [J]. Journal of Alloys and Compounds, 2013, 577: s408−s412.

[22] WANG X, CHEN Y, XU L, LIU Z, WOO K D. Effects of Sn content on the microstructure, mechanical properties and biocompatibility of Ti−Nb−Sn/hydroxyapatite biocomposites synthesized by powder metallurgy [J]. Materials & Design, 2013, 49: 511−519.

[23] OGHBAEI M, MIRZAEE O. Microwave versus conventional sintering: A review of fundamentals, advantages and applications [J]. Journal of Alloys and Compounds, 2010, 494(1): 175−189.

[24] DAS S, MUKHOPADHYAY A, DATTA S, BASU D. Prospects of microwave processing: An overview [J]. Bulletin of Materials Science, 2009, 32(1): 1−13.

[25] ROY R, AGRAWAL D, CHENG J, GEDEVANISHVILI S. Full sintering of powdered-metal bodies in a microwave field [J]. Nature, 1999, 399(6737): 668−670.

[26] XU J, BAO L, LIU A, JIN X, TONG Y, LUO J, ZHONG Z, ZHENG Y. Microstructure, mechanical properties and superelasticity of biomedical porous NiTi alloy prepared by microwave sintering [J]. Materials Science and Engineering C, 2015, 46: 387−393.

[27] YANG D, GUO Z, SHAO H, LIU X, JI Y. Mechanical properties of porous Ti−Mo and Ti−Nb alloys for biomedical application by gelcasting [J]. Procedia Engineering, 2012, 36: 160−167.

[28] MOUR M, DAS D, WINKLER T, HOENIG E, MIELKE G, MORLOCK M M, SCHILLING A F. Advances in porous biomaterials for dental and orthopaedic applications [J]. Materials, 2010, 3(5): 2947−2974.

[29] BANSIDDHI A, SARGEANT T, STUPP S I, DUNAND D. Porous NiTi for bone implants: A review [J]. Acta Biomaterialia, 2008, 4(4): 773−782.

[30] RYAN G, PANDIT A, APATSIDIS D P. Fabrication methods of porous metals for use in orthopaedic applications [J]. Biomaterials, 2006, 27(13): 2651−2670.

[31] GEETHA M, SINGH A, ASOKAMANI R, GOGIA A. Ti based biomaterials, the ultimate choice for orthopaedic implants—A review [J]. Progress in Materials Science, 2009, 54(3): 397−425.

[32] NAGELS J, STOKDIJK M, ROZING P M. Stress shielding and bone resorption in shoulder arthroplasty [J]. Journal of Shoulder and Elbow Surgery, 2003, 12(1): 35−39.

[33] NIINOMI M. Metallic biomaterials [J]. Journal of Artificial Organs, 2008, 11(3): 105−110.

[34] NOURI A. Novel metal structures through powder metallurgy for biomedical applications [D].Victoria: Deakin University, 2008.

[35] NOURI A, HODGSON P D, WEN C E. Biomimetic porous titanium scaffolds for orthopaedic and dental applications [M]. Victoria: In Tech, 2010.

[36] ÖZGEN C. Production and characterization of porous titanium alloys [D]. Ankara: Middle East Technical University, 2007.

[37] WEN C, MABUCHI M, YAMADA Y, SHIMOJIMA K, CHINO Y, ASAHINA T. Processing of biocompatible porous Ti and Mg [J]. Scripta Materialia, 2001, 45(10): 1147−1153.

[38] BRAM M, STILLER C, BUCHKREMER H P, STÖVER D, BAUR H. High−porosity titanium, stainless steel, and superalloy parts [J]. Advanced Engineering Materials, 2000, 2(4): 196−199.

[39] WEN C E, YAMADA Y, NOURI A, HODGSON P D. Porous titanium with porosity gradients for biomedical applications [J]. Materials Science Forum, 2007, 539: 720−725.

[40] DEWIDAR M M, LIM J. Properties of solid core and porous surface Ti−6Al−4V implants manufactured by powder metallurgy [J]. Journal of Alloys and Compounds, 2008, 454(1): 442−446.

[41] ZHANG Y, LI D, ZHANG X. Gradient porosity and large pore size NiTi shape memory alloys [J]. Scripta Materialia, 2007, 57(11): 1020−1023.

[42] RAUSCH G, BANHART J. Handbook of cellular metals [M]. Weinheim: Wiley−VCH Verlag, 2002: 21−28.

[43] KIM Y W, LEE Y J, NAM T H. Shape memory characteristics of Ti−Ni−Mo alloys sintered by sparks plasma sintering [J]. Journal of Alloys and Compounds, 2013, 577: s205−s209.

[44] XU J, BAO L, LIU A, JIN X, LUO J, ZHONG Z, ZHENG Y. Effect of pore sizes on the microstructure and properties of the biomedical porous NiTi alloys prepared by microwave sintering [J]. Journal of Alloys and Compounds, 2015, 645: 137−142.

[45] BECKER W, LAMPMAN S. Fracture appearance and mechanisms of deformation and fracture [J]. Materials Park, OH: ASM International, 2002: 559−586.

[46] PADULA II S, SHYAM A, RITCHIE R, MILLIGAN W. High frequency fatigue crack propagation behavior of a nickel-base turbine disk alloy [J]. International Journal of Fatigue, 1999, 21(7): 725−731.

[47] PEART R, TOMLIN D. Diffusion of solute elements in beta-titanium [J]. Acta Metallurgica, 1962, 10(2): 123−134.

[48] GIBBS G, GRAHAM D, TOMLIN D. Diffusion in titanium and titanium−niobium alloys [J]. Philosophical Magazine, 1963, 92(8): 1269−1282.

[49] KIM H, IKEHARA Y, KIM J, HOSODA H, MIYAZAKI S. Martensitic transformation, shape memory effect and superelasticity of Ti−Nb binary alloys [J]. Acta Materialia, 2006, 54(9): 2419−2429.

[50] CHAI Y, KIM H, HOSODA H, MIYAZAKI S. Self-accommodation in Ti−Nb shape memory alloys [J]. Acta Materialia, 2009, 57(14): 4054−4064.

[51] CHAVES J, FLORÊNCIO O, SILVA P, MARQUES P, AFONSO C. Influence of phase transformations on dynamical elastic modulus and anelasticity of beta Ti−Nb−Fe alloys for biomedical applications [J]. Journal of the Mechanical Behavior of Biomedical Materials, 2015, 46: 184−196.

[52] HON Y H, WANG J Y, PAN Y N. Composition/phase structure and properties of titanium-niobium alloys [J]. Materials Transactions, 2003, 44(11): 2384−2390.

[53] HAN M K, KIM J Y, HWANG M J, SONG H J, PARK Y J. Effect of Nb on the microstructure, mechanical properties, corrosion behavior, and cytotoxicity of Ti−Nb alloys [J]. Materials, 2015, 8(9): 5986−6003.

[54] MURRAY J L. The Nb−Ti (niobium−titanium) system [J]. Bulletin of Alloy Phase Diagrams, 1981, 2(1): 55−61.

[55] KIM H Y, MIYAZAKI S. Martensitic transformation and superelastic properties of Ti−Nb base alloys [J]. Materials Transactions, 2015, 56(5): 625−634.

[56] GUO Y, GEORGARAKIS K, YOKOYAMA Y, YAVARI A. On the mechanical properties of TiNb based alloys [J]. Journal of Alloys and Compounds, 2013, 571: 25−30.

[57] KIM H Y, HASHIMOTO S, KIM J I, HOSODA H, MIYAZAKI S. Mechanical properties and shape memory behavior of Ti−Nb alloys [J]. Materials Transactions, 2004, 45(7): 2443−2448.

[58] HORIUCHI Y, NAKAYAMA K, INAMURA T, KIM H Y, WAKASHIMA K, MIYAZAKI S, HOSODA H. Effect of Cu addition on shape memory behavior of Ti−18mol%Nb alloys [J]. Materials Transactions, 2007, 48(3): 414−421.

[59] HAO Y, LI S, SUN S, YANG R. Effect of Zr and Sn on Young's modulus and superelasticity of Ti–Nb-based alloys [J]. Materials Science and Engineering A, 2006, 441(1): 112−118.

[60] INAMURA T, SHIMIZU R, KIM J I, KIM H Y, WAKASHIMA K, MIYAZAKI S, HOSODA H. Rolling texture of α''-phase in Ti−22mol%Nb−3mol%Al biomedical shape memory alloy [J]. Materials Science Forum, 2007, 561: 1517−1520.

[61] SHARMA B, VAJPAI S K, AMEYAMA K. Microstructure and properties of beta Ti−Nb alloy prepared by powder metallurgy route using titanium hydride powder [J]. Journal of Alloys and Compounds, 2016, 656: 978−986.

[62] GAO Z, LI Q, HE F, HUANG Y, WAN Y. Mechanical modulation and bioactive surface modification of porous Ti–10Mo alloy for bone implants [J]. Materials & Design, 2012, 42: 13−20.

[63] CHURCHILL C, SHAW J, IADICOLA M. Tips and tricks for characterizing shape memory alloy wire: Part 3—Localization and propagation phenomena [J]. Experimental Techniques, 2009, 33(5): 70−78.

[64] GUO Y. beta-bcc and amorphous Ti-based biocompatible alloys for human body implants [D]. Saint-Martin-d′Héres: Université Grenoble Alpes, 2014.

[65] KOLLI R P, JOOST W J, ANKEM S. Phase stability and stress-induced transformations in beta titanium alloys [J]. JOM, 2015, 67(6): 1273−1280.

微波烧结生物医用多孔 Ti−23%Nb 形状记忆合金的参数优化

Mustafa K. IBRAHIM[1], E. HAMZAH[1], Safaa N. SAUD[2], E. M. NAZIM[1], A. BAHADOR[1]

1. Faculty of Mechanical Engineering, Universiti Teknologi Malaysia, 81310 UTM Johor Bahru, Johor, Malaysia;
2. Faculty of Information Sciences and Engineering,
Management & Science University, 40100 Shah Alam, Selangor, Malaysia

摘　要：采用微波烧结法成功制备多孔 Ti−23%Nb(摩尔分数)形状记忆合金(SMAs)(不含造孔剂)。研究微波烧结对合金显微组织、相组成、相变温度、力学性能和形状记忆效应的影响。结果表明，烧结时间和温度对合金密度和孔隙度大小的影响较大，在 900 °C 下烧结 30 min 的 Ti−23%Nb SMA 具有最小的孔径和最均匀的孔形状。多孔 Ti−Nb SMA 的显微组织主要含有针状和片状的 α''、α 和 β 相，且体积分数随烧结时间和温度不同而变化。由于 β 相稳定元素的含量较高，因此 β 相含量最多，而 α 和 α''相的含量较少。900 °C 烧结 30 min 的样品呈现最优的极限强度和应变，而 1200 °C 烧结 30 min 的样品则具有最高的超弹性。这些合金的弹性模量较低，可以避免“应力屏蔽”效应。因此，微波加热可以应用于烧结生物医用 Ti 合金并提高其力学性能。

关键词：生物医用 Ti−23%Nb 合金；微波烧结；显微组织；相变温度；力学性能

(Edited by Wei-ping CHEN)